AAPS Open

RESEARCH Open Access

PEGylated magnetic nanographene oxide for targeted delivery of arsenic trioxide and sec-o-glucosylhamaudol in tumor treatment with improved dual-drugs synergistic effect

Jinlai Cheng[1], Kun Hong[1], Jianhui Sun[1], Hongmei Li[1], Yu Zhao[1], Qinghe Zhao[1], Yuqing Tan[1] and Miyi Yang[1*]

Abstract

Arsenic trioxide (ATO) is a promising chemotherapeutic agent, but its clinical application is limited due to its poor pharmacokinetics and dose-limited toxicity. Moreover, the combination of ATO and sec-o-glucosylhamaudol (SOG) can improve the therapeutic effect of hepatoma. In this study, PEGylated magnetic nanographene oxide (PEG@MGO) was used as magnetic carriers to enhance the targeting ability of the drug delivery system. ATO and SOG are loaded on the surface of PEG@MGO nanoparticles through electrostatic interactions. This biocompatible nanocomposite shows magnetic susceptibility, pH sensitivity, and high loading capacity of the drugs. The in vitro cytotoxicity study of human hepatoma cell line (HepG2) cells showed more significant cytotoxicity and obvious synergistic effect between ATO and SOG compared with that of single drug-loaded nanoparticles via MTT assay. In vitro cellular uptake was observed by Prussian blue staining and fluorescently labeling. The results demonstrated a high cellular internalization rate of PEG@MGO. The ATO and SOG co-loaded nanodrug significantly inhibits the growth of tumors in vivo, which might be due to the oxidative stress and proapoptotic effect. This type of multidrug nanocomposite offers a promising alternative for cancer therapy.

Keywords Synergistic effect, Arsenic trioxide, Sec-o-Glucosylhamaudol, Magnetic graphene oxide, Drug-delivery

*Correspondence:
Miyi Yang
myyang@icmm.ac.cn
Full list of author information is available at the end of the article

Springer Open

© The Author(s) 2023. **Open Access** This article is licensed under a Creative Commons Attribution 4.0 International License, which permits use, sharing, adaptation, distribution and reproduction in any medium or format, as long as you give appropriate credit to the original author(s) and the source, provide a link to the Creative Commons licence, and indicate if changes were made. The images or other third party material in this article are included in the article's Creative Commons licence, unless indicated otherwise in a credit line to the material. If material is not included in the article's Creative Commons licence and your intended use is not permitted by statutory regulation or exceeds the permitted use, you will need to obtain permission directly from the copyright holder. To view a copy of this licence, visit http://creativecommons.org/licenses/by/4.0/.

Graphical Abstract

A pH-sensitive polyethylene glycol-modified magnetic graphene oxide loaded with ATO and SOG (PEG@MGO@ATO + SOG) was prepared for the magnetically targeted and efficient synergistic-chemo cancer therapy, which exhibited high specificity and good biocompatibility.

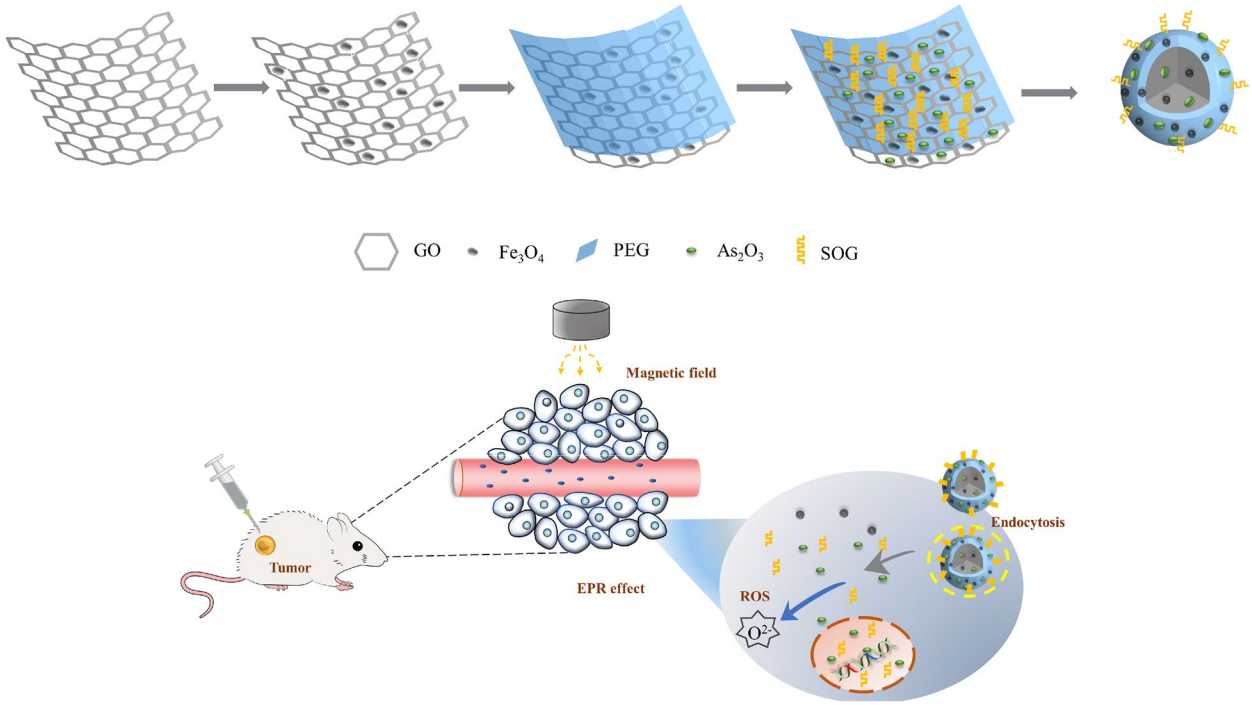

Introduction

Compared with immunotherapy and radiotherapy, chemotherapy is more acceptable, with many alternative chemotherapeutic agents. Nevertheless, effective cancer therapies are still unavailable. The main problem is that chemotherapeutic drugs are toxic to both cancerous and normal cells (Reddy et al. 2005). Hence, an effective and safe drug-delivery system is necessary (Mu et al. 2020). Increasing attention has been paid to the development of nano-drug carriers. Nano-drug carriers with diameters between 10 and 1000 nm work as media to transport chemotherapeutic agents (Gong et al. 2016). This novel drug-delivery system can improve drug solubility, prolong the blood circulation period, and enhance drug accumulation by passive or active targeting, which will help to minimize adverse effects of clinical drugs (Geng et al. 2018; Khursheed et al. 2020).

Natural and synthetic polymeric materials, inorganic materials, and lipids have been used as drug carriers (Karthik et al. 2013; Truong et al. 2013). Graphene is a unique carbon-based nanomaterial, which looks like honeycombs (Balandin 2020). Graphene oxide (GO) is the oxidized form of graphene widely used in the biomedical field. Graphene and its derivatives are biologically safe at the cellular and organic levels, even at relatively high concentrations (Ou et al. 2016). GO has large oxygen-containing functional groups (Allahbakhsh et al. 2013), good hydrophilicity (Tian et al. 2019), huge surface area (Liu et al. 2013), and potentially low manufacturing cost (Kim et al. 2013). Those oxygen-containing groups in GO, like C=O, -COOH, -OH, and -C-O-C, make it easier to be chemically functionalized (Kazempour et al. 2019). The hydrophobic interactions and/or π–π stacking of these functional groups make drug loading possible (Xing et al. 2016; Xing et al. 2016). The above properties facilitate the design of novel nano-carriers based on GO to deliver therapeutic drugs (Priyadarsini et al. 2018; Wang et al. 2018; Pooresmaeil et al. 2018; Abdelhamid et al. 2021).

A magnetic nanoparticle-based drug delivery system can transfer drugs to a certain site under the influence of an external magnetic field (Yang et al. 2018, Feng et al. 2018). Ferroferric oxide (Fe_3O_4) is an ideal choice to prepare the magnetic drug delivery system for its paramagnetism, and there is no magnetization after removing the

magnetizing field. Besides, reversible magnetism can prevent the aggregation of nanoparticles, which can enhance the stability of nanomedicines. Generally, the application of Fe_3O_4 in vivo requires surface modifications to prevent exocytosis and increase biocompatibility.

Polyethylene glycol (PEG) is one of the most widely studied superhydrophilic polymers and surface modifiers. PEG is cheap, versatile, non-toxic, highly water-soluble, biocompatible, and can transport nanomolecules. Because of its appropriate pharmacokinetics and tissue distributions, the usage of PEG in pharmaceuticals is approved by the Food and Drug Administration (FDA). The accumulation of nanoparticles modified with PEG (PEGylation) in liquids decreased compared with that of nanoparticles without PEG. Moreover, PEG will increase the internal circulation time and reduce excretion via the reticuloendothelial system (RES) (Tas et al. 2021). Thus, PEGylated magnetic nanographene oxide (PEG@MGO) is a potential nano-carrier to deliver hydrophobic drugs in biological systems (Deb et al. 2018; Ma et al. 2020).

Arsenic trioxide (ATO) is a traditional Chinese medicine known as the "king of poisons" with a lethal dose value (LD_{50}) of 15 mg/kg (rat, oral) (Vogt 2017). The usage of ATO was significantly reduced in the past century due to the public's fear of its toxicity (Evens et al. 2004). In the late twentieth century, ATO became popular again. It was approved by the FDA as the frontline therapy for acute promyelocytic leukemia (APL) in 2000 (Hoonjan et al. 2018), and it was also approved for the treatment of newly diagnosed APL by the European Medicines Agency (EMA) in 2016 (European Medicines Agency 2016). Subsequently, ATO was proven effective in other hematological malignancies, such as acute myeloid leukemia, chronic myelogenous leukemia, and Hodgkin's disease (Swindell et al. 2013). With the blood clearance efficacy, ATO powder was not suitable for solid tumors therapy. Several attempts have been made to develop ATO's anticancer properties by increasing its bioavailability and reducing systemic toxicity. These methods include sensitizing carcinoma cells before ATO treatment, combining ATO therapy with other conventional chemotherapeutic agents, and developing ATO-loaded nano-drugs (Wang et al. 2012). Henceforth, ATO has become a "potential broad-spectrum anti-cancer drug" (Akhtar et al. 2017). Hepatocellular carcinoma (HCC) is one of the most malignant cancers and has caused substantial mortality worldwide (Bray et al. 2018, Yang et al. 2019). HCC is insensitive to adriamycin and platinum chemotherapeutics, so the development of ATO-loaded nano-drugs will provide new treatment options for liver cancer.

Synergism and detoxication are important principles of traditional Chinese medicines. We try to find some new combinations of ATO under the guidance of these principles. The ancient Chinese books named "YanFangHuiJi" and "JiJiuBianFang" recorded that the root of the traditional Chinese medicine, Radix Saposhnikoviae, can significantly reduce ATO toxicity. In addition, modern pharmacological research show this traditional Chinese medicine can protect the liver from oxidization (Jiang et al. 2014). What is more, we find sec-O-glucosylhamaudol (SOG), a compound extracted from Radix Saposhnikoviae, expressing anti-cancer enhancement of ATO in in vitro and in vivo experiments.

We introduce a novel nano-drug, controlled-release nano-magnetic carrier, based on Fe_3O_4 nanoparticles and GO nanosheets, which was conjugated with ATO and SOG to improve the therapeutic efficacy of HCC. The drug cargo was constituted of PEG-modified Fe_3O_4 as hydrophilic corona and GO as a hydrophobic core. The morphology, size, microstructure, and magnetic properties of the nanoparticles were examined. A series experiments were implemented, and the results demonstrated that ATO and SOG could be released in a controlled manner in targeted lesions. This nano platform represents a new approach for the treatment of HCC.

Experimental methods

Materials

Graphene oxide (GO) was purchased from XFNANO (Nanjing, China). Ferric chloride hexahydrate ($FeCl_3{\cdot}6H_2O$), ferrous chloride tetrachloride ($FeCl_2{\cdot}4H_2O$), trisodium citrate dihydrate ($Na_3C_6H_5O_7{\cdot}2H_2O$), arsenic trioxide (ATO), and polyethylene glycol (PEG, average MV 400) were purchased from Sinopharm Chemical Reagent Co., Ltd. (Shanghai, China). sec-O-Glucosylhamaudol (SOG) was bought from Chengdu Biopurify Phytochemicals Ltd. (Chengdu, China). All the materials mentioned were used without further purification.

Dulbecco's modified Eagle's medium (DMEM) was purchased from HyCone (Logan, UT, USA). Fetal bovine serum (FBS) was obtained from Sijiqing (Hangzhou, China). A total of 0.25% trypsin-EDTA solution, 3(4,5-dimethylthiazol-2-yl)-2,5-diphenyl tetrazolium bromide (MTT), Prussian blue iron staining kit (with Eosin solution), dimethyl sulfoxide (DMSO), double antibiotic (streptomycin/penicillin), phosphate buffer solution (PBS, pH 7.4), fluorescein isothiocyanate, and sodium dodecyl sulfate were obtained from Solarbio (Beijing, China). The Annexin V-FITC/PI Apoptosis Detection Kit was purchased from Becton, Dickinson, and Company (San Digo, USA), and 2′, 7′-dichlorodihydrofluorescein diacetate (DC-FHDA) was bought from Sigma-Aldrich, USA.

Cell line and cell culture

The human hepatoma cell line (HepG2) and human hepatocyte cell line (L02) were purchased from Shanghai Cell Bank, Chinese Academy of Sciences (Shanghai, China). Both cells were cultivated in a CO_2 incubator (Thermo Scientific, USA). HepG2 and L02 were cultured in a DMEM medium supplemented with fetal bovine serum (10%, v/v), penicillin (100 UI/mL), and streptomycin (100 UI/mL). When the cell confluence reached nearly 80%, the cells were digested and passaged with 0.25% trypsin for subsequent experiments.

Preparation of Fe_3O_4 and polyethylene glycol-modified magnetic GO (PEG@MGO)

The preparation for PEG@MGO was according to previous reports with some developments (Wang et al. 2018; Mao et al. 2019). GO powder (20 mg) was poured into 50 mL purified water with 2 g PEG-400 and sonicated for 1 h. Then, 2.162 g $FeCl_3 \cdot 6H_2O$ and 0.795 g $FeCl_2 \cdot 4H_2O$ were added. The suspension was stirred and maintained at 60 °C for 30 min with N_2 protection to generate magnetic cores according to reaction 1. After that, sodium hydroxide (NaOH) solution (1 mol/L) was dropwise added until the pH value to 11. Then, 0.247 g sodium citrate dihydrate ($C_6H_5Na_3O_7$) was added under constant magnetic stirring. The temperature of the mixture was kept at 60 °C and stirred for 2 h. The precipitation was collected by magnetic separation. After being washed three times with water and ethanol, the black nanoparticles were dried in the vacuum oven at 60 °C for 6 h.

$$Fe^{2+} + 2Fe^{3+} + 8OH^- \rightarrow Fe_3O_4 + 4H_2O$$

Reaction 1: The preparation of Fe_3O_4

Characterization

Fourier transform infrared (FTIR) spectra were recorded on a Nicolet Ncxus 670 FTIR spectrometer (Thermo Scientific, USA) in the range of 500–4000 cm^{-1} by the KBr pellet technique. X-ray powder diffraction (XRD) data were collected in the range of $2\theta = 4 - 90°$ using a Rigaku XRD S2 powder diffractometer (Rigaku Corporation, Japan). Morphological evaluation of the freeze-dried nanoparticles was recorded by a Tescan mira3 field emission scanning electron microscope (FE-SEM, Tescan, Czech Republic). The magnetic property of nanoparticles was measured by the vibrating sample magnetometer (VSM) using Lakeshore 730T (Lakeshore, USA). Dynamic light scattering (DLS) analysis was performed on a Nano-ZetaSizer ZEN3600 (Malvern, UK).

Preparation of drug-loaded PEG-Fe_3O_4@GO

In order to evaluate the adsorption process, different formulations were prepared. ATO and SOG co-loaded PEG@MGO (PEG@MGO@ATO + SOG) were prepared as follows: 10 mg PEG@MGO was added into 10 mL ethyl alcohol solution containing 2 mg/mL ATO and 4 mg/mL SOG. ATO-loaded PEG@MGO (PEG@MGO@ATO) was prepared in the solution containing 2 mg/mL ATO only, while SOG-loaded PEG@MGO (PEG@MGO@SOG) was prepared in the solution containing 4 mg/mL SOG only. These resulting mixtures were stirred at 50 °C for 6 h, and then the nanoparticles were collected via an Nd magnet and washed with double distilled water and ethanol three times in sequence to remove unabsorbed ATO and SOG. Finally, the above drug-loaded nanoparticles were freeze-dried at − 20 °C for 24 h. The method of ATO and SOG loading on PEG@MGO was optimized through preliminary experiments based on the solubility of SOG and inhibition rates of HepG2.

After drug loading, the supernatant was collected and filtered via a 0.22 μm membrane filter. The concentrations of ATO and SOG in the supernatant were determined through an inductively coupled plasma emission spectrum (ICP 6300, Thermo Electron Corporation, USA) and high-performance liquid chromatography (HPLC 1100, Shimadzu, Japan), respectively. Detailed analytical methods were showed in supporting information. Drug encapsulation efficiency (EE%) and drug content (DC%) of PEG@MGO@ATO + SOG and PEG@MGO@ATO were calculated according to Eqs. (1) and (2), respectively.

$$EE\% = \frac{\text{Amount of drug in nanoparticles}}{\text{Amount of drug added}} \times 100\% \quad (1)$$

$$DC\% = \frac{\text{Amount of drug in nanoparticles}}{\text{Amount of nano} - \text{carrier}} \times 100\% \quad (2)$$

In vitro drug release

The release behaviors of SOG and ATO on PEG@MGO were investigated at different pH conditions. Briefly, 10 mg drug-loaded nanoparticles were dispersed in 10 mL buffer solution with different pH values (pH 5.0, 6.8, and 7.4) and given to continuous shaking at 37 °C. At desired time intervals, 1 mL released solution was taken from the stirring dissolution medium. Subsequently, an equal amount of fresh buffer saline was added to the original media. The percent of released ATO and SOG was calculated according to the following formula:

$$\text{Release}(\%) = \frac{\text{W released dose}}{\text{W loaded dose}} \times 100\% \quad (3)$$

where $W_{\text{released dose}}$ represents the weight of drug released into solution from the drug-loaded nanoparticles; $W_{\text{loaded dose}}$ represents the weight of drug loaded on nanoparticles.

Examine of stability

The residual moisture content was studied for the PEG@MGO and PEG@MGO@ATO + SOG which were newly prepared and stored after 30 days. The residual moisture content was measured by Karl Fischer titration using a Mettler DL 38 titrator (Mettler-Toledo, Switzerland). 100.0 mg samples of the above nanoparticles were used for the analysis and the measured moisture content was expressed in percentage. What is more, the dispersive capacity of PEG@MGO after 30 days' storage over 25 °C /60RH and 40 °C /75RH was detected by dispersing 10 mg PEG@MGO into 10mL water.

Cellular uptake of nano-drug carriers

The cellular uptake of the nano-drug was analyzed by Prussian blue staining and a fluorescence microscope.

To perform Prussian blue staining, the following steps were made. HepG2 was seeded in 12-well plates at a density of 1×10^5 cells/well and incubated for 24 h (37 °C ,5% CO_2). Then the cells were treated differently. One group was only treated with PEG@MGO at a concentration of 15 μg/mL in DMEM medium for 4 h. The other group was treated with PEG@MGO at a concentration of 15 μg/mL in DMEM medium for 4 h and a small Nd permanent magnet was placed under each well during the first 1 h of incubation. After treatment, cells were fixed with 4% paraformaldehyde for 30 min and then were stained by freshly-prepared Prussian blue staining solution for 30 min and counterstained by eosin for 1 min.

To perform microscopic inspection, HepG2 cells were seeded into a 6-well plate (4×10^5 cells/well). After 24 h, the DMEM medium containing FITC and PEG@MGO/FITC was added to replace the previous solution. FITC and PEG @MGO in the medium were 10 μg/mL and 15 μg/mL, respectively. After being incubated at different times, the cells were washed three times with sterilized PBS and fixed by 75% absolute alcohol. The cells were finally observed and recorded by an inverted fluorescence microscope (DMI3000B, Leica, Germany).

In vitro cytotoxicity and cell apoptosis analysis

The in vitro cytotoxicity of the PEG@MGO on HepG2 and L02 was studied using the MTT assay. These cells were seeded in 96-well plates at a density of 1×10^4 cells/well and incubated for 24 h (37 °C, 5% CO_2). After removing the culture medium, 200 μL DMEM medium containing different concentrations of nanoparticles was added. Following 48 h incubation, the DMEM culture medium was replaced by MTT solution, and these cells were further cultured for 4 h. DMSO (150 μL) was subsequently added to dissolve the formazan crystals formed. The absorbance (OD) values of different groups at 570 nm were recorded by a microplate reader (Multiskan MK3, Thermo Electron Corporation, USA). The measured OD values of the blank, control, and experimental groups were defined as OD_b, OD_c, and OD_e. Cell survival rates were calculated according to Eq. (4). Data are presented as mean ± standard deviation (n = 6).

$$\text{Survival rate}(\%) = \frac{OD_e - OD_b}{OD_c - OD_b} \times 100\% \tag{4}$$

For cell apoptosis assay, cells were seeded in 6-well plates at a density of 2×10^5 cells/well. After 24 h of incubation, nano-drugs at different concentrations were added to the cell medium, and the cells were incubated for another 24 h. Then, the cells were harvested, washed twice with cold PBS, and stained with 5 μL Annexin V-FITC and 5 μL PI for 15 min at room temperature in the dark. These cells were resuspended in 200 μL binding buffer and were analyzed using flow cytometry (FACSVerse, Becton, Dickinson and Company, USA).

Combination effect of SOG and ATO

Tumor-cell proliferation-inhibition behaviors of SOG and ATO against HepG2 were evaluated. The concentrations of ATO and SOG ranged from 0.5 to 64 μmol/L and from 16 to 2048 μmol/L, respectively. In the combination group, the drug concentrations are the same as the above, the combination effects of SOG and ATO loaded on PEG@MGO were also explored. The concentrations of PEG@MGO@ATO, PEG@MGO@SOG, and PEG@MGO@ATO + SOG ranged from 2.5 to 120 μg/mL. After the cells were incubated for 24 h, 48 h, and 72 h under drug application, the cell survival rates were detected by the microplate reader at 570 nm by MTT assay and the process showed above. CI_{50} was measured according to Chou's method (Chou 2006).

$$CI_n = \frac{D_1}{(D_n)_1} + \frac{D_2}{(D_n)_2}$$

In the equation, where $(Dn)_1$ and $(Dn)_2$ represent the IC_{50} value when drug 1 or 2 works singly. D_1 and D_2 represent the concentrations of drug 1 and drug 2 when given simultaneously at the IC_{50} value. $CI_{50} > 1$ was used to indicate antagonism between two drugs, $CI_{50} = 1$, the additive effect, and $CI_{50} < 1$, synergism.

Cellular reactive oxygen species (ROS) measurements

The released intracellular ROS in different groups was measured using DCFH-DA. HepG2 cells were seeded

in 6-well plates with a density of 4×10^5 cells/well and were incubated at 37 °C for 24 h. Then, the cells were incubated with free ATO, the mixture of ATO and SOG, PEG@MGO@ATO, and PEG@MGO@SOG + ATO for 24 h. The concentration of nanoparticles was 15 μg/ml and the amount of ATO and SOG added are equal to the amount of drugs loaded on nanoparticles. At the end of the cultivation, the collected cells were resuspended in a DMEM medium containing DCHF-DA (10 μM) at 37 °C for 30 min. The cells were washed with serum-free culture solution three times to remove the DCFH-DA that did not enter the cells. Then, the fluorescence was measured by flow cytometry (excitation at 485 nm and emission at 530 nm).

In vivo tumor inhibition

Twenty-eight 6-week-old male BALB/c nude mice were bought from Beijing Vital River Laboratory Animal Technology Co., Ltd. (Beijing, China). Approximately 2×10^6 HepG2 cells dispersed in 0.2 mL saline solution were injected subcutaneously into the right flank region of every mouse. When the volume of tumors approached 100 mm^3 (about 10 days after the tumor inoculation), the tumor-bearing mice were randomly divided into four groups (7 mice /group) for different treatments. The therapy method for groups were listed as follows: (1) inject saline solution via the tail vein; (2) inject PEG@MGO@SOG + ATO at a dose of 20 mg/kg via the tail vein, then fix an external magnet on the back of the tumor with glues; (3) inject free ATO at a dose of 5 mg/kg via the tail vein; (4) inject PEG@MGO@SOG + ATO at 20 mg/kg via the tail vein. The initial body weight was recorded and monitored every 3 days before treatment. The tumor size was determined and calculated by the formula $V = a \times b^2/2$, where a and b were the longest and shortest diameters of the tumor, respectively. Mice were sacrificed on the 18th day after treatment, the tumors were excised for weighing. Then, tumors and main organs (heart, liver, spleen, lung, and kidney) were fixed in 10% formalin, followed by hematoxylin and eosin (H&E) staining assay.

Statistical analysis

Data were processed using Spss.20 (SPSS Inc., Chicago, USA) and presented as mean ± standard deviation (SD). Statistical analysis was performed using a one-way analysis of variance (ANOVA). The difference was regarded as statistically significant when $P \leq 0.05$. Statistic software Graph-pad Prism 5.0 (GraphPad Software, California, USA) was used for all graphical illustrations.

Results and discussion

Characterizations of the nanoparticles

Figure 1a shows the FTIR spectrums of GO, PEG@MGO, and PEG@MGO@ATO + SOG. The peaks of the GO sample at 3650 cm^{-1}, 1500 cm^{-1}, and 1075 cm^{-1} are related to -OH stretching, C-O stretching vibration, epoxy, and alkoxy, respectively. The peak at 1650 cm^{-1} was attributed to C-C stretching vibration. The characteristic peak of the PEG@MGO sample at 945 cm^{-1} was caused by the $-CH_2$ groups in PEG. Additionally, the absorption peaks of -OH stretching at 3600 cm^{-1} and 3050 cm^{-1} contributed to -CH group bands, which confirmed the successful attachment of PEG to GO surface. The peaks at 530 cm^{-1} related to vibrations of Fe-O show the successful modification of Fe_3O_4. The FTIR spectrums of PEG@MGO@ATO + SOG are similar to those of PEG@MGO, which means the ATO and SOG loading will not affect the nano-carrier structure (Farani et al. 2020; Dong et al. 2010).

The presence of different compositions was verified with XRD analysis. Figure 1B exhibits the crystalline phases of GO, Fe_3O_4, and PEG@MGO. The peak of the PEG@MGO at $2\theta = 11.29°$ is related to 002 diffractions of GO flakes. Peaks at $2\theta = 30.23°$, 37.23°, 41.22°, 57.15°, 66.91° display the typical peaks of cubic spinel Fe_3O_4 NPs. This suggests the remaining of the inner core structure even after modification. DLS analysis was used to evaluate the size and particle distributions of Fe_3O_4. As shown in Fig. S1, the average particle diameter for Fe_3O_4 was 150 nm for a volume. The PDI value was 0.179 showed a great homogeneity of this magnetic nanoparticle.

Figure 1c and e shows the SEM images of different nanocomposites. As shown in Fig. 1c, the GO has a sheet-like structure with smooth surfaces and a wrinkled edge. After the modification with the Fe_3O_4 and PEG400, the SEM image of the nanocomposites revealed the regular spherical morphology (Fig. 1d). Figure 1e shows the image of ATO- and SOG-loaded nanoparticles. The rough surface may be attributed to the adsorption of drugs on the surface of the PEG@MGO. In conclusion, the modified GO sheets can prevent the restacking of GO sheets and enlarge the surface area to absorb active drugs.

The magnetic properties of Fe_3O_4, PEG@MGO, and PEG@MGO@ATO + SOG were studied by the magnetic hysteresis loop, which is shown in Fig. 2a. The saturation magnetization value of Fe_3O_4, PEG@MGO, and PEG@MGO@ATO + SOG was 61.1, 41.4, and 16.1 emu/g, respectively. The above results demonstrate the good superparamagnetic ability of the nano-drug with no coercivity or remanence (Atacan et al. 2015; Cheng et al. 2018). The insert picture shows the good water

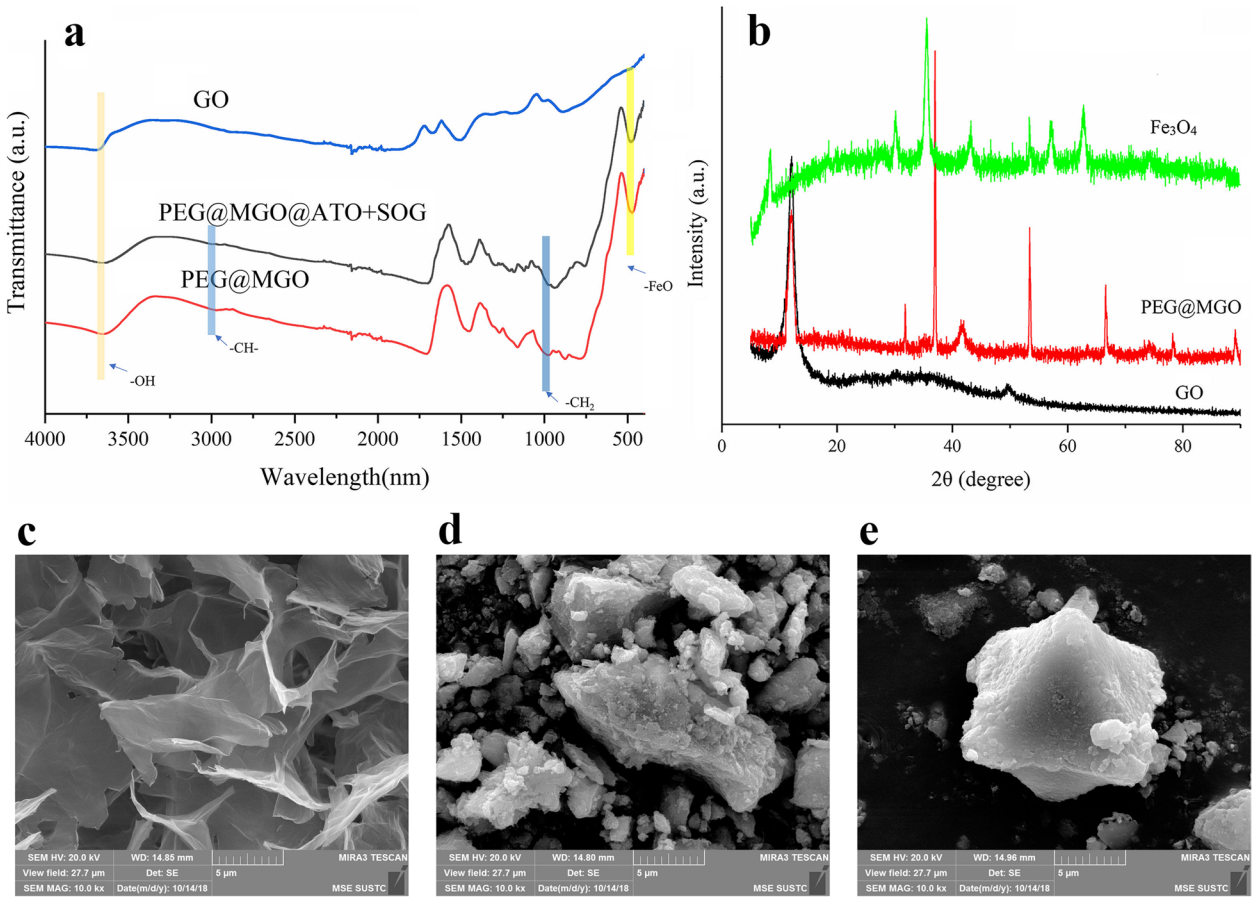

Fig. 1 **a** FT-IR spectra of GO, PEG@MGO, and PEG@MGO@ATO + SOG. **b** X-ray diffraction patterns of GO, Fe_3O_4, and PEG@MGO. SEM image of GO (**c**), PEG@MGO (**d**), and PEG @ MGO@ATO + SOG (**e**)

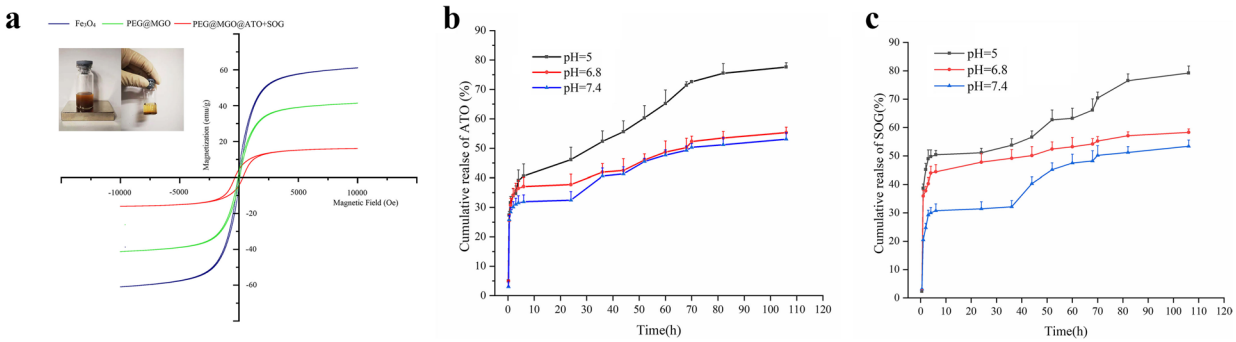

Fig. 2 **a** Magnetization curves of Fe_3O_4, PEG@MGO, and PEG@MGO@ATO + SOG, magnetic recovery of PEG@MGO@ATO + SOG from aqueous solution (insert). **b**, **c** Release profile of ATO and SOG from PEG@MGO@ATO + SOG at different pH values

dispersibility and easy magnetic separation of the PEG@MGO@ATO + SOG.

Drug loading and in vitro release study

Drug loading capacity is a very important factor in evaluating the therapeutic effect of nanodrugs. The loading of ATO and SOG mainly depended on the electrostatic interaction between drugs and the PEG@MGO. The EE% and DC% of PEG@MGO@ATO and PEG@MGO@ATO + SOG were listed in Table 1. These data demonstrated the good drug encapsulation efficiency of the PEG@MGO nanocomposites. This phenomenon can

Table 1 Drug loading ability of different nanoparticles

	PEG@MGO@ATO	PEG@MGO@ATO + SOG	
	ATO	ATO	SOG
EE(%)	14.76 ± 3.2	18.03 ± 4.2	38.25 ± 3.8
DC(%)	29.89 ± 2.6	36.52 ± 5.0	153.00 ± 4.2

be explained as the addition of PEG on the surface of the dendrimer can prevent the diffusion of drugs to the solution. In addition, the high loading capacity might be related to the high surface area of the nanocomposites. Also, the EE% and DC% of the combination drugs are higher than those of only ATO-loaded nano-drug. It may be explained as positively charged PEG@MGO naturally absorbs the negatively charged ATO and the addition of SOG can produce covalent interaction between two drugs to enhance the drug loading efficiency.

The release profiles of ATO and SOG from PEG@MGO@ATO + SOG at pH 5.0, 6.8, and 7.4 are shown in Fig. 2b and c. The drug release rates of ATO from PEG@MGO@ATO + SOG with the three pH values were close during the initial 6 h. The results showed that the cumulative release rate of ATO from PEG@MGO@ATO + SOG reached up to 77.6% ± 1.5%, 55.3.00% ± 1.9%, and 53.1% ± 2.2% at pH 5.0, 6.8, and 7.4 respectively after 108 h. The releasing rule of SOG was similar to that of ATO. After 108 h, the cumulative release rate of SOG from PEG@MGO@ATO + SOG was approximately 79.21% ± 2.5%, 58.3% ± 1.2%, and 53.4% ± 2.2% at pH 5.0 6.8, and 7.4, respectively. These results show that the release of ATO and SOG from nanocarrier is pH-sensitive and the release rate increased with the decrease of pH values. The addition PEG enhances the hydrophilic nature of the dendrimer thus improving its stability. Under acidic conditions, the hydrogen bonds are stronger than those occurring at pH 7.4. Therefore, the high release of ATO and SOG from PEG@MGO@ATO + SOG nanocomposite under acidic pH conditions indicates the potential application of the proposed nanocarrier in cancer treatment.

Stability of nanoparticles

The residual moisture content of PEG@MGO and PEG@MGO@ATO + SOG were showed in Table 2. It is well known that the residual moisture content plays important roles in determining a power's long-term stability, both physically and chemically. The results showed the moisture content of the both two nanoparticles were less than 1.2% which can prove the stability of PEG@MGO whether it loads drug or not. Meanwhile, the dispersibility of PEG@MGO remains nearly unchanged regardless the store condition (Fig. S3).

Table 2 Residual moisture content of the nanoparticles after different storage time and determined by Karl Fischer titration (mean ± SD; $n = 3$)

Formulations	Residual moisture (%)	
	Newly prepared	After 30 days storage
PEG@MGO	0.52 ± 0.01	1.01 ± 0.2
PEG@MGO@ATO + SOG	0.63 ± 0.11	1.06 ± 0.3

In vitro cellular uptake

Cellular internalization is essential for nanoparticles used as drug carriers. Prussian blue staining, which selectively stains Fe^{3+}, can be used to evaluate the endocytosis behaviors of PEG@MGO. Figure 3 shows that blue dots accumulated in cells after being treated with the magnetic drug carrier, indicating that PEG@MGO could be uptaken by tumor cells. What is more, the intracellular amount of PEG@MGO was significantly increased by an external Nd-magnet (Fig. 3c, d). These results indicated that a magnetic field would enhance the endocytosis of PEG@MGO.

To investigate the motion law of the nano-carrier, PEG@MGO was labeled with FITC (green) for subcellular observation. Green fluorescence appeared after 4 h co-culture and was widely distributed in the cells after 24 h co-culture, which is shown in Fig. 3e. This revealed that PEG@MGO exhibited a high level of cell uptake through endocytosis in a time-dependent manner.

Cytotoxicity assay and cellular apoptosis analysis

For the potential biomedical applications, it is necessary to investigate the cytotoxicity of nano-carriers. Figure 4 showed the results for cells treated with PEG@MGO for 48 h and with drugs loaded with inhibition effect, respectively. It should be noticed that the viability of the tumor cells (HepG2) and liver cells (L02) were observed to be larger than ~ 70% even at higher concentration of 250 μg/mL after 48 h (Fig. 4a, b), indicating the excellent biocompatibility of blank nano-carriers. ATO- and SOG-loaded PEG@MGO showed cell inhibition to HepG2 cells and L02 cells, while the inhibition effect of L02 is lower than that of HepG2. The results implied that the PEG@MGO nanoparticles have minor toxicity and great selectivity as a drug delivery in cancer treatment.

Annexin V/PI staining was carried out to investigate the influence of various concentrations of the novel nanodrug on the apoptosis rates of HepG2 cells. The apoptosis rates of cells treated with PEG@MGO@ATO + SOG under 10 μg/mL, 15 μg/mL, 20 μg/mL, 25 μg/mL, and 50 μg/mL were studied, respectively. After the incubation of 24 h, the apoptosis rates were 13.5%, 16.0%,17.9%,

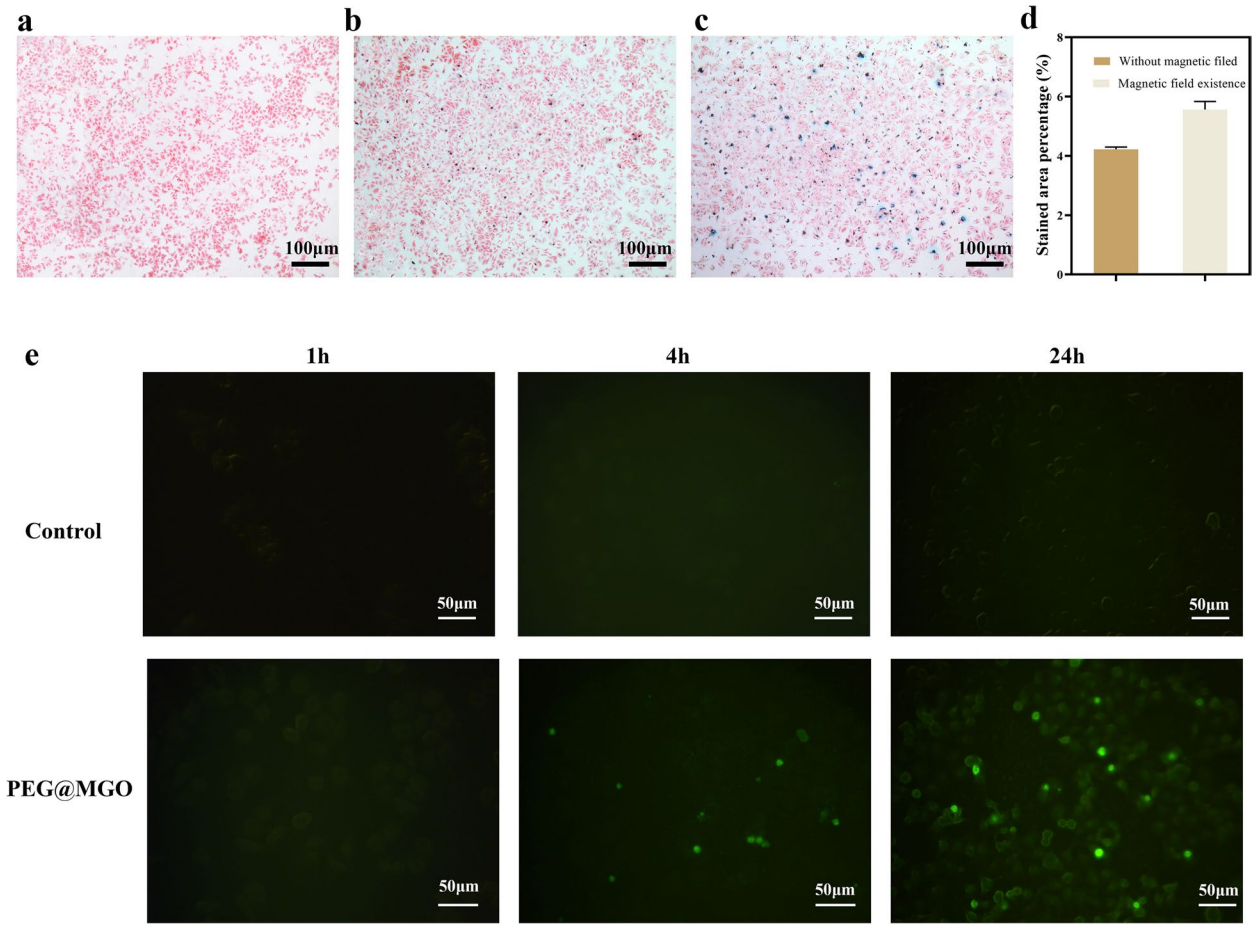

Fig. 3 Cellular uptake of PEG@MGO. Images of HepG2 stained with Prussian blue: **a** cells with no treatment, **b** treated with 15 μg/ml PEG@MGO for 4 h, **c** treated with 15 μg/ml PEG@MGO under the magnetic field for the first 1 h. **d** Area percentage analysis after staining with Prussian blue. **e** Microscopy images of HepG2 incubation with FITC-labeled PEG@MGO after different time

19.2% and 21.3% in Fig. 5a. The results demonstrate that the inhibitory activity of the nano-drug increased with the increase of its concentrations and the cellular apoptosis of HepG2 cells caused by PEG@MGO@ATO + SOG was a concentration dependent manner (Fig. 5b). It can be also hypothesized that PEG@MGO@ATO + SOG will inhibit tumor proliferation by triggering the apoptotic path way of cancer cells.

Cytotoxicity and synergism

The cytotoxicity of free drugs and drug-loaded nanoparticles on HepG2 cells was measured by the MTT assay. The IC_{50} values of free drugs, co-drugs, drug-loaded PEG@MGO, and combination index (CI) values of co-drugs were summarized in Tables 3 and 4. The results show that the cytotoxicity of all experimental groups is dose-and time-dependent. Compared with single-drug treatment, dual-drug combination treatment exhibits higher cytotoxicity. The CI values of SOG + ATO after 24 h, 48 h, and 72 h incubation were 0.714, 0.83, and 0.964, respectively. The CI values smaller than 1 indicated the synergistic effect of SOG and ATO. The inhibition ratios of HepG2 at different combination concentrations of ATO and SOG shown in Fig. S4 added evidence of the cell growth inhibition under the combination usage of SOG and ATO. The IC_{50} values of PEG@MGO@ATO + SOG were smaller than those of PEG@MGO@SOG and PEG@MGO@ATO. From the above results, we can conclude that the active targeting of PEG@MGO@ATO + SOG leads more drug molecules to enter tumor cells to inhibit tumor growth.

Cellular ROS analysis

To investigate whether the novel nano-drug causes oxidative stress in cancer cells, ROS levels of HepG2 cells were measured by flow cytometry after being incubated with different formulations (Fig. 5c). The results showed that the intracellular ROS levels were significantly

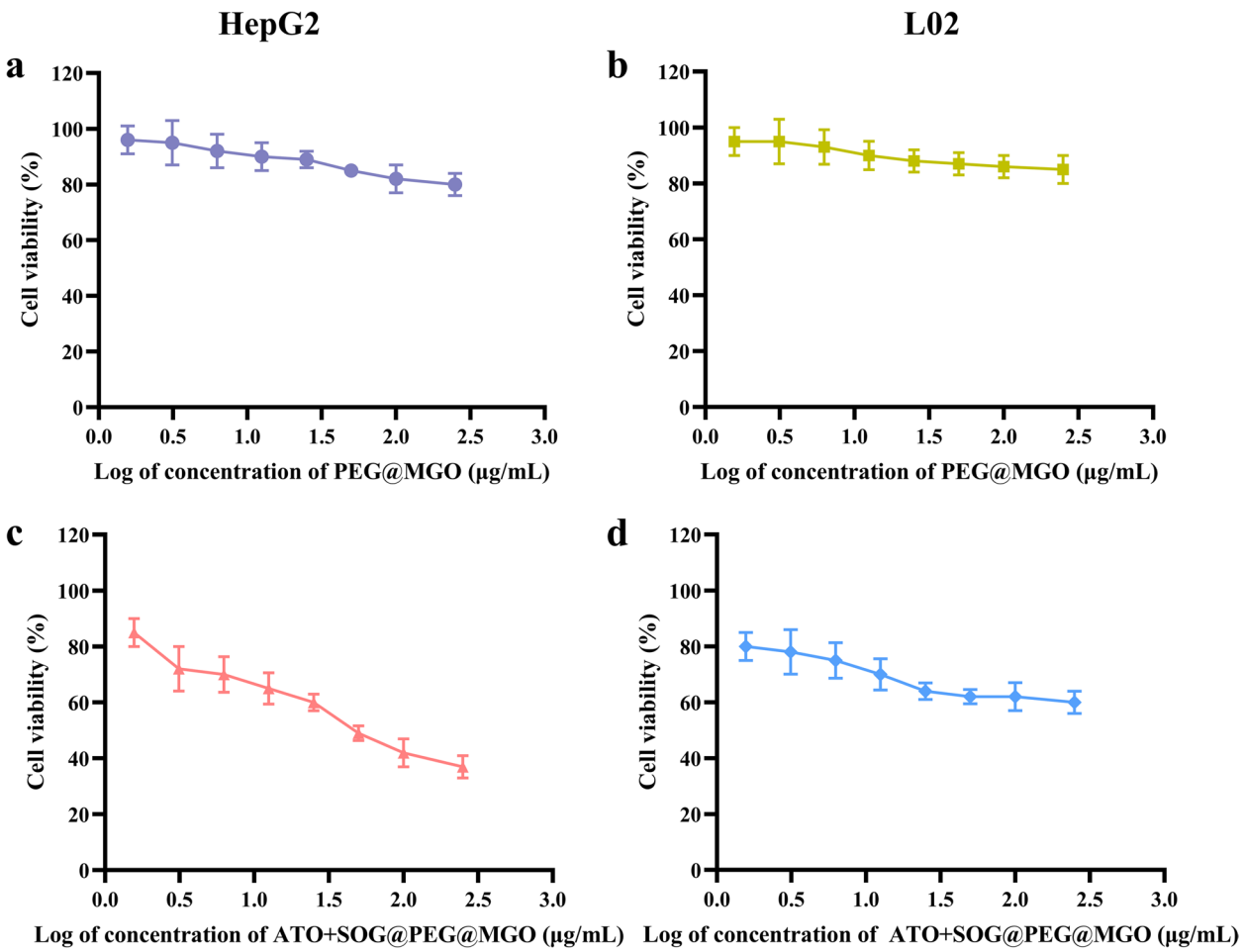

Fig. 4 Cytotoxicity of PEG@MGO against **a** HepG2 cells and **b** L02 cells after incubation. Cytotoxicity of ATO + SOG@ PEG@MGO against **c** HepG2 cells and **d** L02 cells after incubation

increased after 24 h's drug treatment. The intracellular ROS levels in ATO + SOG and PEG@MGO@ATO + SOG groups were higher than those in the groups of ATO and PEG@MGO@ATO, which is due to the synergistic effect. The intracellular ROS levels in PEG@MGO@ATO and PEG@MGO@ATO + SOG groups increased 2.30-fold and 2.59-fold, respectively, as compared with those of the free ATO group. The values of those two groups increased 1.46-fold and 1.59-fold compared with those of the ATO + SOG group. A significant increase in ROS level was observed in the cells when treated with a co-drug. Excessive intracellular ROS may induce oxidative stress in mitochondria and destruction of the integrity of the mitochondria membrane structure and finally, induce cellular apoptosis and death. PEG@MGO@ATO + SOG was more likely to produce ROS than other drugs, which may be ascribed to its sustained drug release manner.

In vivo synergistic anti-cancer effect

Based on the effective therapy of the nanocomposite in vitro, a HepG2 xenograft model was established by intravenous administration with different formulations to study the synergistic efficacy. As shown in Fig. 6a, the volume of tumor showed significant differences among different groups. Treatment with ATO led to a slight inhibition of HepG2 tumor growth compared to the PBS group. The group treated with PEG@MGO@ATO + SOG under a magnetic field displayed the most significant tumor growth inhibition, outperforming both the group of free ATO and PEG@MGO@ATO. After 18 days of observation, tumor tissues were extracted, weighed, and photographed. Tumor weights were 95.2, 476.2, and 226.1 mg in the group of magnet + PEG@MGO@ATO + SOG, ATO, and magnet + PEG@MGO@ATO, respectively, as compared with 707.5 mg of the PBS group. The average tumor weight of the PEG@MGO@

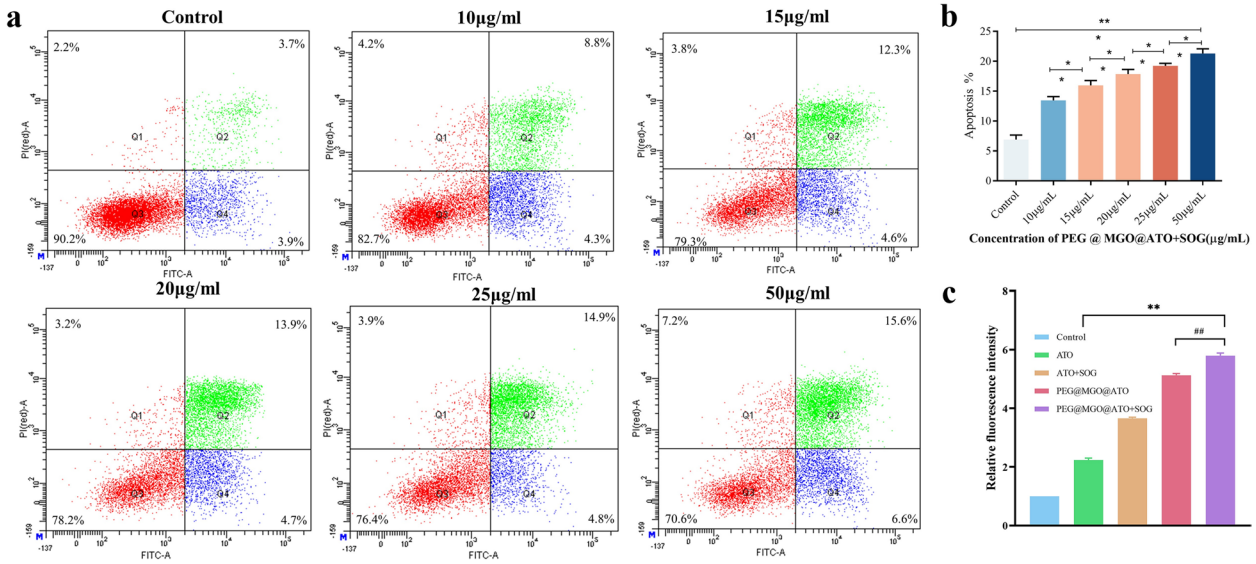

Fig. 5 The apoptosis rates of HepG2 cells after incubation with PEG@MGO@ATO + SOG at different concentrations. **a** Flow cytometry analysis via Annexin V/PI staining and **b** quantitative analysis of tumor cells apoptosis. $^{*}P < 0.05$, $^{**}P < 0.01$, $^{***}P < 0.001$. **c** Effect of different treatment on the production of intracellular ROS according to relative fluorescence intensity. Compared with ATO treated group, $^{**}P < 0.01$; compared with ATO + SOG treated group, $^{\#\#}P < 0.01$

Table 3 IC_{50} and CI of SOG and ATO against HepG2 cells for different incubation time

Time	IC_{50} drug alone (95% confidence interval)		IC_{50} drug combination (95% confidence interval)		CI at IC_{50}
	SOG(μmol/L)	ATO(μmol/L)	SOG(μmol/L)	ATO(μmol/L)	
24 h	1575.0 ± 59.5	52.0 ± 2.8	586.8 ± 33.0	17.8 ± 1.7	0.71
48 h	773.9 ± 36.6	19.9 ± 2.1	289.8 ± 27.2	9.9 ± 1.4	0.83
72 h	458.5 ± 18.5	14.2 ± 2.4	219.6 ± 16.1	6.9 ± 0.3	0.96

Table 4 IC_{50} of different formulations against HepG2 cells for different incubation time

Time	Nanodrugs	IC_{50}(μg/mL)
24 h	PEG@MGO@SOG	87.41 ± 1.84
	PEG@MGO@ATO	51.87 ± 4.73
	PEG@MGO@ATO + SOG	27.07 ± 0.86
48 h	PEG@MGO@SOG	78.89 ± 2.55
	PEG@MGO@ATO	41.69 ± 2.22
	PEG@MGO@ATO + SOG	21.91 ± 1.78
72 h	PEG@MGO@SOG	68.99 ± 1.78
	PEG@MGO@ATO	30.89 ± 0.66
	PEG@MGO@ATO + SOG	15.62 ± 0.84

ATO + SOG group was much lower than those of the other groups (Fig. 6b). The pictures of the tumors among the different groups are consistent with the results of the tumor growth curve, tumor weight (Fig. 6d), and in vitro experiments. The tumor growth in mice treated with PBS showed a fast and unrestrained tendency, and the final volume was about 11-fold of the initial size. The free ATO could not prevent tumor growth might because of the quick dilution of fluid flow.

H&E staining examinations of the tumor tissues after treatment are displayed in Fig. 6e; it appeared that the tumor tissue displayed a typical necrotic response after treatment; the cell necrosis of PEG@MGO@ATO + SOG under magnet was the most obvious. All these indicate that the nano-drug PEG@MGO@ATO + SOG owns a remarkable tumor inhibition effect, and the magnetic microenvironment may promote the accumulation of the anti-cancer drug in tumor cells.

The possible toxicity of the formulations was also studied. As shown in Fig. 6c, no significant reduction in body weight was observed in the different groups during the treatment period, indicating the high biocompatibility

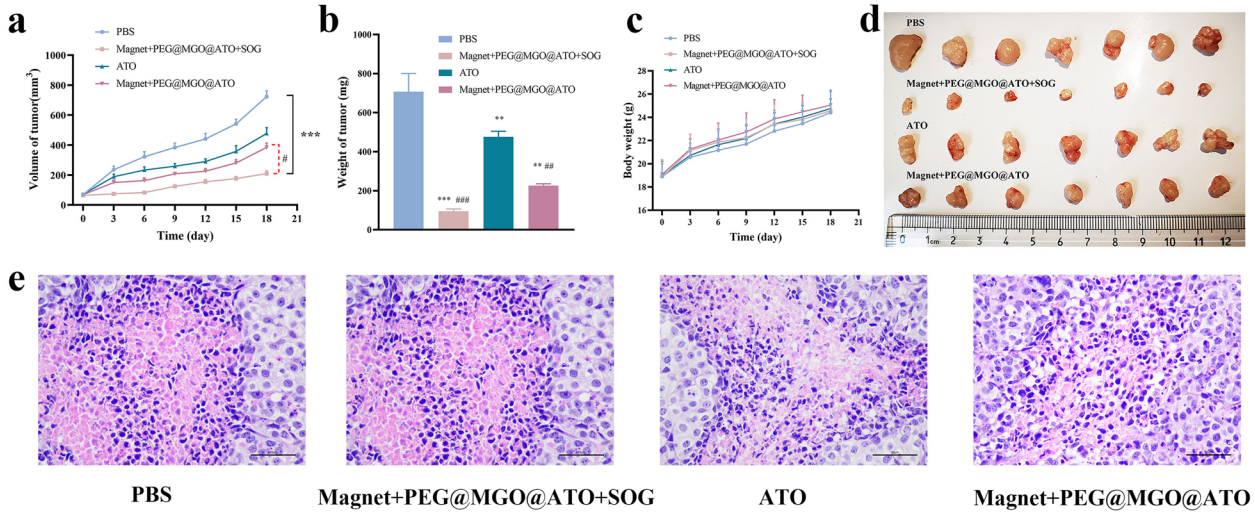

Fig. 6 In vivo tumor inhibitory effects on HepG2 xenograft tumors. **a** Tumor volumes were measured every three days. Compared to PBS group, $^{***}p < 0.001$; compared to magnet + PEG@MGO@ATO group, $^{\#}p < 0.05$. **b** Weight of tumors of each therapeutic group after 18 days of treatments. Compared to PBS group, $^{***}p < 0.001$. $^{**}p < 0.01$; compared to ATO group, $^{\#\#}p < 0.01$. $^{\#\#\#}p < 0.001$. **c** The body weight of mice in treatments. **d** The optical image of the excised tumor tissues after 18 days of treatments. **e** The H&E analysis for different groups (scale bar: 50 μm)

of these PEG@MGO-based nano-drugs. H&E stained images of major organs (heart, spleen, lung, and kidney) shown in Fig. S5, revealing nearly no difference in pathological lesions of varied groups. These results collectively indicated that the nanoparticles did not cause appreciable systemic toxicity or an inflammatory response.

Conclusion

In summary, a pH-sensitive polyethylene glycol-modified magnetic graphene oxide loaded with ATO and SOG (PEG@MGO@ATO + SOG) was first prepared for the magnetically targeted and efficient synergistic-chemo cancer therapy. This new biocompatible drug delivery system was prepared by coating hollow Fe_3O_4 nanoparticles on the surface of GO sheets via electrostatic interaction and then immobilized with hydrophilous PEG-400. The combination of ATO and SOG, the active ingredient of traditional Chinese medicines, can improve the inhibition of HepG2. These two drugs were loaded on the nano-carrier due to the large surface area of the PEG@MGO. The nanocomposite exhibited excellent magnetic hyperthermia effect, controlled drug release, and pH sensitivity, which could be used for accurate cancer therapy. Furthermore, it showed excellent anti-cancer performance in vitro and vivo experiments. The results showed that this ATO- and SOG-co-loaded nanodrug exhibited high potential in the HCC adjuvant therapy.

Abbreviations

APL	Acute promyelocytic leukemia
ATO	Arsenic trioxide
CI	Combination index
DC-FHDA	2′, 7′-Dichlorodihydrofluorescein diacetate
DC%	Drug content
DMSO	Dimethyl sulfoxide
DMEM	Dulbecco's modified Eagle's medium
EE%	Drug encapsulation efficiency
EMA	European Medicines Agency
FBS	Fetal bovine serum
FDA	Food and Drug Administration
Fe_3O_4	Ferroferric oxide
FTIR	Fourier transform infrared spectra
$FeCl_3{\cdot}6H_2O$	Ferric chloride hexahydrate
HepG2	Human hepatoma cell line
HCC	Hepatocellular carcinoma
HPLC	High-performance liquid chromatography
GO	Graphene oxide
LD50	Lethal dose value
L02	Human hepatocyte cell line
MTT	4,5-Dimethylthiazol-2-yl-2,5-diphenyl tetrazolium bromide
PEG	Polyethylene glycol
PEG@MGO	PEGylated magnetic nanographene oxide
RES	Reticuloendothelial system
ROS	Reactive oxygen species
SEM	Scanning emission microscope
SOG	Sec-o-Glucosylhamaudol
VSM	Vibrating sample magnetometer
XRD	X-ray powder diffraction

Supplementary Information

The online version contains supplementary material available at https://doi.org/10.1186/s41120-023-00079-4.

Additional file 1: Fig. S1. DLS result of Fe_3O_4 nanoparticles. **Fig. S2.** TEM image of Fe_3O_4 nanoparticles. **Fig. S3.** Photos of PEG@MGO dispersed in water. A. PEG@MGO stored over 25℃/60%RH for 30 days; B. PEG@MGO stored over 40℃/75% for 30 days. **Fig. S4.** The inhibition ratios of HepG2 at different combination concentrations of ATO and SOG after 48h co-culture. **Fig S5.** H&E histology images of the major organs in mice after administration of (A) PBS, (B) Magnet+PEG@MGO@ATO+SOG, (C) ATO, (D) Magnet+PEG@MGO@ATO for 18 days.

Authors' contributions
Jinlai Cheng: performed laboratory experiments, analyzed, interpreted data, and wrote the first copy of the manuscript. Kun Hong: contributed to the experiments. Jianhui Sun: co-write, revised the manuscript, and provided the final approval of the version to publish. Hongmei Li: contributed to the design of the work, supervised the research, and provided the final approval of the version to publish and agreed to be accountable for all aspects of the work. Yuqing Tan: supervised the project. Miyi Yang: put the design of the work, contributed in revision, analysis, interpretation of data and provided financial support of this project. All authors discussed the results and contributed to the final manuscript. The author(s) read and approved the final manuscript.

Declarations

Availability of data and materials
The datasets used and/or analyzed during the current study are available from the corresponding author on reasonable request.

Competing interests
The authors declare no conflict of interests.

Funding
This work was financially supported by the Fundamental Research Funds for the Central public welfare research institutes (ZZ13-YQ-056).

Acknowledgements
Not applicable.

Authors' information
Not applicable.

Author details
[1]China Academy of Chinese Medical Sciences Institute of Chinese Materia Medica, Dongzhimen Nei Ave. Nanxiaojie 16#, Dongcheng District, Beijing 100700, China.

Received: 15 December 2022 Accepted: 8 May 2023
Published online: 05 June 2023

References

Abdelhamid HN, Hussein KH (2021) Graphene oxide as a carrier for drug delivery of methotrexate. Biointerface Res App 11(6):14726–14735
Akhtar A, Wang SX, Ghali L, Bell C, Wen X (2017) Recent advances in arsenic trioxide encapsulated nanoparticles as drug delivery agents to solid cancers. J Biomed Res 31(3):177–188
Allahbakhsh A, Sharif F, Mazinani S (2013) The influence of oxygen-containing functional groups on the surface behavior and roughness characteristics of graphene oxide. NANO 08(04):1350044
Atacan K, Ozacar M (2015) Characterization and immobilization of trypsin on tannic acid modified Fe_3O_4 nanoparticles. Colloids Surf B Biointerfaces 128:227–236
Balandin AA (2020) Phononics of graphene and related materials. ACS Nano 14(5):5170–5178
Bray F, Ferlay J, Soerjomataram I, Siegel RL, Torre LA, Jemal A (2018) Global cancer statistics 2018: GLOBOCAN estimates of incidence and mortality worldwide for 36 cancers in 185 countries. CA Cancer J Clin 68(6):394–424
Cheng M, Wang Z, Lv Q, Li C, Sun S, Hu S (2018) Preparation of amino-functionalized Fe_3O_4@mSiO_2 core-shell magnetic nanoparticles and their application for aqueous Fe^{3+} removal. J Hazard Mater 341:198–206
Chou T (2006) Theoretical basis, experimental design, and computerized simulation of synergism and antagonism in drug combination studies. Pharmacol Rev 58(3):621–681
Deb A, Vimala R (2018) Camptothecin loaded graphene oxide nanoparticle functionalized with polyethylene glycol and folic acid for anticancer drug delivery. J Drug Deliv Sci Tec 43:333–342
Dong H, Zhao Z, Wen H, Li Y, Guo F, Shen A, Pilger F, Lin C, Shi D (2010) Poly(ethylene glycol) conjugated nano-graphene oxide for photodynamic therapy. Sci China Chem 53(11):2265–2271
Evens AM, Tallman MS, Gartenhaus RB (2004) The potential of arsenic trioxide in the treatment of malignant disease: past, present, and future. Leuk Res 28(9):891–900
European Medical Agency (2016) Trisenox EMEA/H/C000388/II/0058 assessment report
Farani MR, Khadiv–Parsi P, Riazi GH, Ardestani MS, Rad HS (2020) PEGylation of graphene/iron oxide nanocomposite: assessment of release of doxorubicin, magnetically targeted drug delivery and photothermal therapy. Appl Nanosci 10(4):1205–1217
Feng L, Xie R, Wang C, Gai S, He F, Yang D, Lin J (2018) Magnetic targeting, tumor microenvironment responsive intelligent nanocatalysts for enhanced tumor ablation. ACS Nano 12:11000–11012
Geng S, Wu L, Cui H, Tan W, Chen T, Chu PK, Yu XF (2018) Synthesis of lipid-black phosphorus quantum dot bilayer vesicles for near-infrared-controlled drug release. Chem Commun 54(47):6060–6063
Gong R, Chen G (2016) Preparation and application of functionalized nano drug carriers. Saudi Pharm J 24(3):254–257
Hoonjan M, Jadhav V, Bhatt P (2018) Arsenic trioxide: insights into its evolution to an anticancer agent. J Biol Inorg Chem 23(3):313–329
Jiang C, Li W, Zheng Y (2014) Protective effect of Saposhnikovia divaricata extract on liver. J Jilin Agricultural Univ 36(3):3
Karthik S, Puvvada N, Kumar BN, Rajput S, Pathak A, Mandal M, Singh ND (2013) Photoresponsive coumarin-tethered multifunctional magnetic nanoparticles for release of anticancer drug. ACS Appl Mater Interfaces 5(11):5232–5238
Kazempour M, Namazi H, Akbarzadeh A, Kabiri R (2019) Synthesis and characterization of PEG-functionalized graphene oxide as an effective pH-sensitive drug carrier. Artif Cells Nanomed Biotechnol 47(1):90–94
Khursheed R, Singh SK, Wadhwa S, Gulati M, Awasthi A (2020) Enhancing the potential preclinical and clinical benefits of quercetin through novel drug delivery systems. Drug Discov Today 25(1):209–222
Kim NH, Kuila T, Lee JH (2013) Simultaneous reduction, functionalization and stitching of graphene oxide with ethylenediamine for composites application. J Mater Chem A 1(4):1349–1358
Liu J, Cui L, Losic D (2013) Graphene and graphene oxide as new nanocarriers for drug delivery applications. Acta Biomater 9(12):9243–9257
Ma C, Hu J, Sun W, Ma Z, Yang W, Wang L, Zhang H (2020) Graphene oxide-polyethylene glycol incorporated PVDF nanocomposite ultrafiltration membrane with enhanced hydrophilicity, permeability, and antifouling performance. Chemosphere 253:126649
Mao ND, Jeong H, Nguyena TKN, Nguyene TML, Doa TVV, Thuc CNH, Perréb P, Ko SC, Kim HG, Tran DT (2019) Polyethylene glycol functionalized graphene oxide and its influences on properties of poly(lactic acid) biohybrid materials. Compos Part B: Eng 161:651–658
Mu W, Chu Q, Liu Y, Zhang N (2020) A review on nano-based drug delivery system for cancer chemoimmunotherapy. Nanomicro Lett 12(1):142
Ou L, Song B, Liang H, Liu J, Feng X, Deng B, Shao L (2016) Toxicity of graphene-family nanoparticles: a general review of the origins and mechanisms. Part Fibre Toxicol 13(1):57
Pooresmaeil M, Namazi H (2018) β-Cyclodextrin grafted magnetic graphene oxide applicable as cancer drug delivery agent: synthesis and characterization. Mater Chem Phys 218:62–69
Priyadarsini S, Mohanty S, Mukherjee S, Basu S, Mishra M (2018) Graphene and graphene oxide as nanomaterials for medicine and biology application. J Nanostructure Chem 8(2):123–137
Reddy LH (2005) Drug delivery to tumours: recent strategies. J Pharm Pharmacol 57(10):1231–1242
Swindell EP, Hankins PL, Chen H, Miodragovic DU, O'Halloran TV (2013) Anticancer activity of small-molecule and nanoparticulate arsenic(III) complexes. Inorg Chem 52(21):12292–12304
Tas A, Keklikcioglu Cakmak N (2021) Synthesis of PEGylated nanographene oxide as a nanocarrier for docetaxel drugs and anticancer activity on prostate cancer cell lines. Hum Exp Toxicol 40(1):172–182
Tian J, Wu S, Yin X, Wu W (2019) Novel preparation of hydrophilic graphene/graphene oxide nanosheets for supercapacitor electrode. Appl Surf Sci 496:143696

Truong NP, Gu W, Prasadam I, Jia Z, Crawford R, Xiao Y, Monteiro MJ (2013) An influenza virus-inspired polymer system for the timed release of siRNA. Nat Commun 4:1902
Vogt J (2017) Stoichiometry and chemical reactions: Exam Survival Guide: Physical. Chemistry Springer, Cham, pp 9–16
Wang X, Deng A, Cao W, Li Q, Wang L, Zhou J, Hu B, Xing X (2018) Synthesis of chitosan/poly (ethylene glycol)-modified magnetic nanoparticles for antibiotic delivery and their enhanced anti-biofilm activity in the presence of magnetic field. J Mater Sci 53:9: 6433–6449
Wang C, Zhang Z, Chen B, Gu L, Li Y, Yu S (2018) Design and evaluation of galactosylated chitosan/graphene oxide nanoparticles as a drug delivery system. J Colloid Interface Sci 516;332–341
Wang S, Wu X, Tan M, GOng J, Tan W, Bian B, Chen M, Wang Y (2012) Fighting fire with fire: Poisonous Chinese herbal medicine for cancer therapy. J Ethnopharmacol 140(1):33–45
Xing R, Jiao T, Liu Y, Ma K, Zou Q, Ma G, Yan X (2016) Co-Assembly of Graphene Oxide and Albumin/Photosensitizer Nanohybrids towards Enhanced Photodynamic Therapy. Polymers 8(5):181
Xing R, Liu K, Jiao T, Zhang N, Ma K, Zhang R, Zou Q, Ma G, Yan, X (2016) An Injectable Self-Assembling Collagen-Gold Hybrid Hydrogel for Combinatorial Antitumor Photothermal/Photodynamic Therapy. Adv Mater 28(19):3669–3676
Yang H, Li Y, Lee D (2018) Multifunctional and Stimuli-Responsive Magnetic Nanoparticle-Based Delivery Systems for Biomedical Applications. Adv Therap 1(2):1800011
Yang JD, Hainaut P, Gores GJ, Amadou A, Plymoth A, Roberts LR (2019) A global view of hepatocellular carcinoma: trends, risk, prevention and management. Nat Rev Gastroenterol Hepatol 16(10):589–604

Publisher's Note

Springer Nature remains neutral with regard to jurisdictional claims in published maps and institutional affiliations.

Submit your manuscript to a SpringerOpen journal and benefit from:

► Convenient online submission
► Rigorous peer review
► Open access: articles freely available online
► High visibility within the field
► Retaining the copyright to your article

Submit your next manuscript at ► springeropen.com